Evolution of turbulent kinetic energy and dissipation rate in near and far field region of a single jet using PIV

Kamran Ghamkhar[1], Stefan Puttinger [1], Micheal Weiß[1], Mahdi Saeedipour[1,*]

1: Department of Particulate Flow Modelling, Johannes Kepler University Linz, Austria
*Corresponding author: mahdi.saeedipour@jku.at

Keywords: Single jets, turbulence decay, time-resolved planer PIV tomographic PIV, dissipation rate.

ABSTRACT

The objective of this study is to characterize the turbulence statistics in the near and far fields of a single turbulent jet driven by a water-pump system. High spatial resolution 2D PIV and high temporal resolution tomographic PIV were equipped to a feasibility analysis and comparison of their performance in measuring the turbulent properties. Mean turbulent kinetic energy, turbulent dissipation rate, and turbulence decay time scale were extracted as results from the time-resolved velocity fields. Also, high temporal resolution in tomographic PIV enables spectral analysis of turbulence evolution in form Power Spectral Density (PSD) of the turbulence velocity fluctuations. The analysis of turbulent properties reveals that the high spatial resolution is crucial for turbulent dissipation rate in 3D measurement. Nevertheless, for kinetic turbulent energy in the far field there is an agreement between 2D and 3D measurements. Besides, experimental observations for turbulent properties in the far field regions are in agreement with existing theoretical power laws including consistency with the well-known -5/3 scaling for fully developed turbulence. The findings provide valuable insights for the design and ongoing construction of the experimental facility for producing homogeneous isotropic turbulence (HIT) in the lab.

1. Introduction

Jet flow is a canonical configuration that has been the focus of extensive experimental investigations in fluid dynamics. The self-similar behavior of the turbulent statistics in this problem has been a subject of interest from the early work in 1989 (George, 1989) to the most recent studies (Kewalramani et al., 2024; Viggiano et al., 2021). In a jet flow, the flow field can be divided into two principal regions, as illustrated schematically in Figure 1. The near field consists of two sub-regions—the potential core and the transitional zone, which are followed downstream by the far field, or fully developed region (Lipari & Stansby, 2011). Previous studies (Ball et al., 2012; Xu & Antonia, 2002) indicate that the axial mean-velocity profile is self-similar form 6 d downstream of the nozzle outlet (where d denotes the nozzle diameter). They mentioned that after self-similarity

in the mean axial velocity profile and turbulent stresses, also the dissipation rate will be self-similar. Most of the studies in the literature have focused on the evolution of the turbulent dissipation rate ε at the centerline, and reported a scaling of $\varepsilon \sim (y/d)^{-4}$, where y is the axial distance (Viggiano et al., 2021; Antonia et al., 1980; Thiesset et al., 2014).

To further investigate these scaling behaviors, advanced velocity measurement techniques are

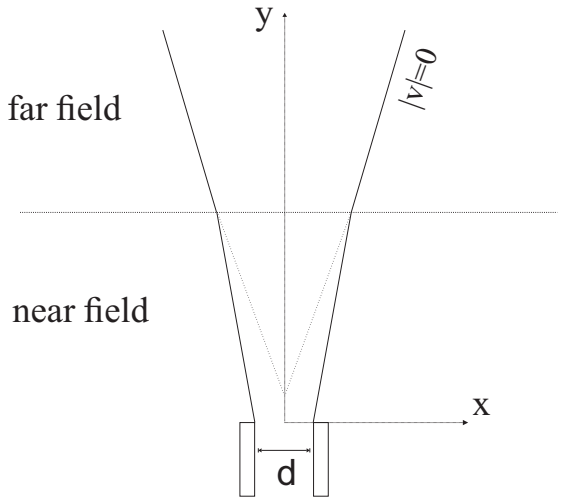


Figure 1. Schematics of a round jet with the indication of near and far fields.

required. Particle Image Velocimetry (PIV) is a robust diagnostic technique, and its application to jet flows enables the extraction of detailed turbulence characteristics, energy budget, vorticity, and shear stresses by resolving the velocity field (Hassanzadeh & Taghavi, 2024). Furthermore, tomographic PIV, due to the three-dimensional nature of turbulence, provides a reliable approach for investigating this problem.

In this study, 2D planar and tomographic PIV setups are employed to extract the turbulence statistics of the flow field up to 40 d downstream the nozzle outlet, with the possibility of comparison between the two methods. Such a systematic study of a single turbulent jet is a prerequisite for further progress in our ongoing efforts to generate homogeneous isotropic turbulence (HIT) in the lab through the random activation of arrays of multiple jets. Of particular interest are the turbulent kinetic energy and dissipation rate in the far field, as well as the vorticity dynamics and its transport across the turbulent length scales. The latter requires spectral analysis within the HIT region. Such analyses are inherently limited by a 2D PIV configuration, whereas tomographic PIV has the potential to provide the volumetric data necessary for this purpose.

The remainder of the paper is structured as follows. Section 2 provides a summary of the experimental setup. Section 3 presents the characterization of the turbulence obtained by the 2D and tomographic PIV measurements. Section 4 contains the conclusion and outlines the future work.

2. Experimental Setup

The designed experimental setup is presented in Figure 2(a). The setup consists of a water pump, an open tank, 2D PIV, and tomographic PIV arrangements. The tank dimensions are 50 cm (width) × 50 cm (length) × 150 cm (height). The bilge pump, with a maximum flow rate of 1.16 L/s, was used to generate the jet flow in this experiment. The pump operation was controlled by PWM modules interfaced through a Controller Area Network (CAN) bus connected via a USB interface (Kvaser Leaf Light v2). The entire control program for regulating pump power was implemented in Python. The Reynolds number at full pump power, based on the nozzle diameter and the centerline mean velocity U_o was 4.75×10^4.
For the 2D PIV measurement, water was seeded with hollow glass spheres with a diameter range of 9-13 μm and density of 1.1 $\mathrm{g/cm^3}$. The illumination of the test section was provided by a 532 nm Nd:YAG pulse laser, which formed a 1 mm thick laser sheet using a set of optical lenses. The images were recorded employing a 16-bit sCMOS camera with a resolution of 2560 × 2160 pixels, operated in double exposure mode at a sampling rate of 10 Hz for 90 seconds. Velocity fields were obtained by processing the image pairs in Davis 11 PIV analysis software. Figure 2(b) shows the experimental setup with 2D PIV arrangements.
For the tomographic PIV setup, four high-speed Phantom VEO cameras equipped with Scheimpflug adapters were arranged as illustrated in Figure 2(c). Each experiment was recorded at 1 kHz for a duration of 5 s, and the measurement sequence was repeated three times. Illumination was provided by two high-power LED-Flashlight units triggered through a LaVision PTU-X synchronization unit. The flow was seeded with fluorescent dye (Rhodamine B) particles with a diameter range of 20-50 μm. For the calibration process, a polynomial mapping function was generated using three planes spaced 20 mm apart in depth. A volumetric self-calibration procedure was carried out within a maximum disparity of 0.15 pixels and an average disparity of 0.04 pixels. Particle reconstruction was performed using the Shake-the-Box algorithm, with a maximum triangulation error of 2 voxels. For velocity-field evaluation, binning was applied using sub-volumes of 128 × 128 × 128 voxels with 75% overlap.

3. Characterization of turbulent properties

In this section, the results obtained by 2D and tomographic PIV are presented. The essential turbulent properties required for the design of a HIT box lab facility, such as turbulent kinetic energy (k), its dissipation rate (ε), and a characteristic time scale indicating the decay of turbulence (τ), are evaluated from the time-resolved velocity measurement.

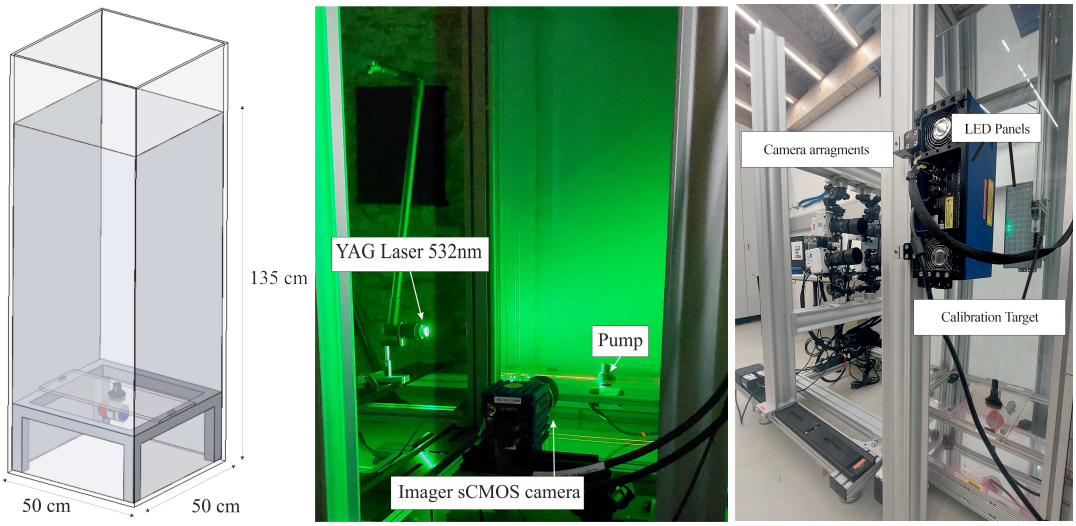


Figure 2. (a) Schematic of experimental setup, (b) 2D PIV measurement, and (c) tomographic PIV.

3.1. Turbulent kinetic energy

Reynolds decomposition expresses the velocity field as a combination of the mean velocity and its fluctuating part, $U_i(x,y,z,t) = \langle U_i(x,y,z,t)\rangle + u_i(x,y,z,t)$, where U_i represents the instantaneous velocity, u_i is the fluctuation about the mean, and $\langle\cdot\rangle$ indicates a time average. Velocity components are denoted by i = 1, 2, 3, corresponding to the x, y, and z directions, respectively. The root mean square (RMS) of the turbulence velocity fluctuations is calculated as $u_i' = \sqrt{\langle u_i^2\rangle}$. Figure 3 presents the root mean square contour of the turbulence fluctuations extracted from the 2D PIV measurement at nine sub-regions downstream. The values of two velocity components along the centerline in the y-direction are plotted in Figure 4(a). The variation of the RMS turbulence velocity fluctuations presented in this diagram is consistent with previous findings reported in Antonia et al. (1980) and Thiesset et al. (2014), and follows the expected far field self-similarity trend, $u_i \sim (y/d)^{-1}$.

Turbulent kinetic energy is defined as the mean kinetic energy per unit mass associated with the velocity fluctuations in a turbulent fluid flow, which is calculated as:

$$k = \frac{1}{2}({u_1'}^2 + {u_2'}^2 + {u_3'}^2) \tag{1}$$

Because of the 2D PIV configuration, only the values of u_1 and u_2 are measurable. Therefore, it is assumed that u_3 is statistically equal to u_1. Figure 4(b) demonstrates the spatial variation of the time-averaged turbulent kinetic energy along the jet centerline. The dashed line represents the theoretical self-preservation scaling, $k \sim (y/d)^{-2}$, and is included as a reference trend. A high degree

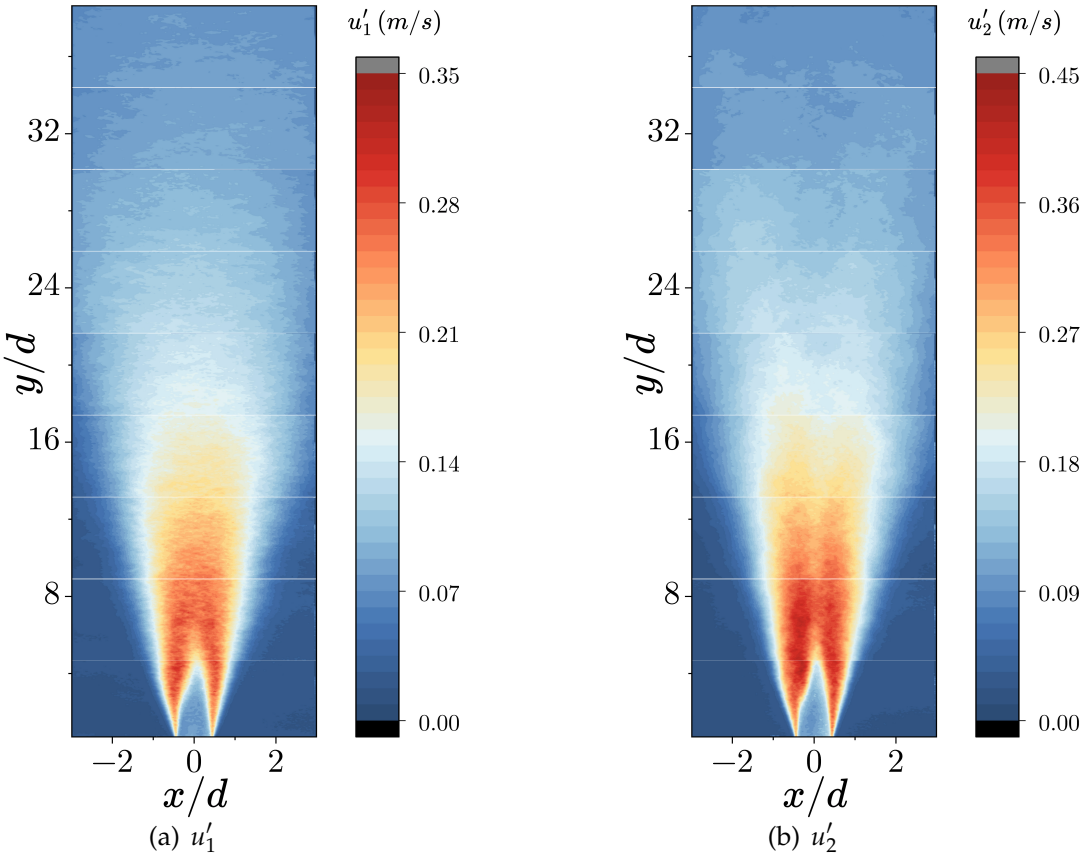


Figure 3. The measured root mean square of the turbulent velocity fluctuations at different sub-regions downstream the jet (a) u_1' and (b) u_2'.

of consistency is observed between the trend line and the experimental data in the far field region at $15 < x/y < 40$.

Using tomographic PIV enabled the reconstruction of the third velocity component (u_3), allowing the turbulent kinetic energy to be evaluated without assumptions. The normalized RMS velocity components, compared with the 2D PIV results, are presented in Figure 5(a). This figure demonstrates that assuming u_3 is statistically equivalent to u_1 along the centerline of a single jet flow is acceptable. Although the reduced spatial resolution of the tomographic PIV leads to an underestimation of the RMS fluctuations in the near field region, the measurements exhibit an agreement with the 2D PIV data in the far field zone ($30 < y/d < 40$). This region, highlighted by the dashed rectangular box in the figure, represents the reliable overlap between the two measurement techniques.

Figure 5(b) presents the normalized, time-averaged turbulent kinetic energy obtained from both 2D PIV and tomographic PIV. The black curve corresponds to the 2D PIV results, whereas the blue curve represents the tomographic PIV data. It is important to note that the 2D PIV measurements were performed with high spatial resolution, and the tomographic PIV system was operated at

lower spatial but higher temporal resolutions. The result of turbulent kinetic energy distribution indicates that, within the region $10 < y/d < 15$, the tomographic PIV under-resolves small-scale eddies, leading to a noticeable deficit in the estimated energy. However, as the flow evolves downstream and the characteristic small-scale structures increase in size, the tomographic PIV results converge toward those obtained from the 2D PIV, particularly in the far field region. As part of the feasibility assessment for extending the present investigation to the HIT box, this far field region is identified as the main domain of interest for the analysis.

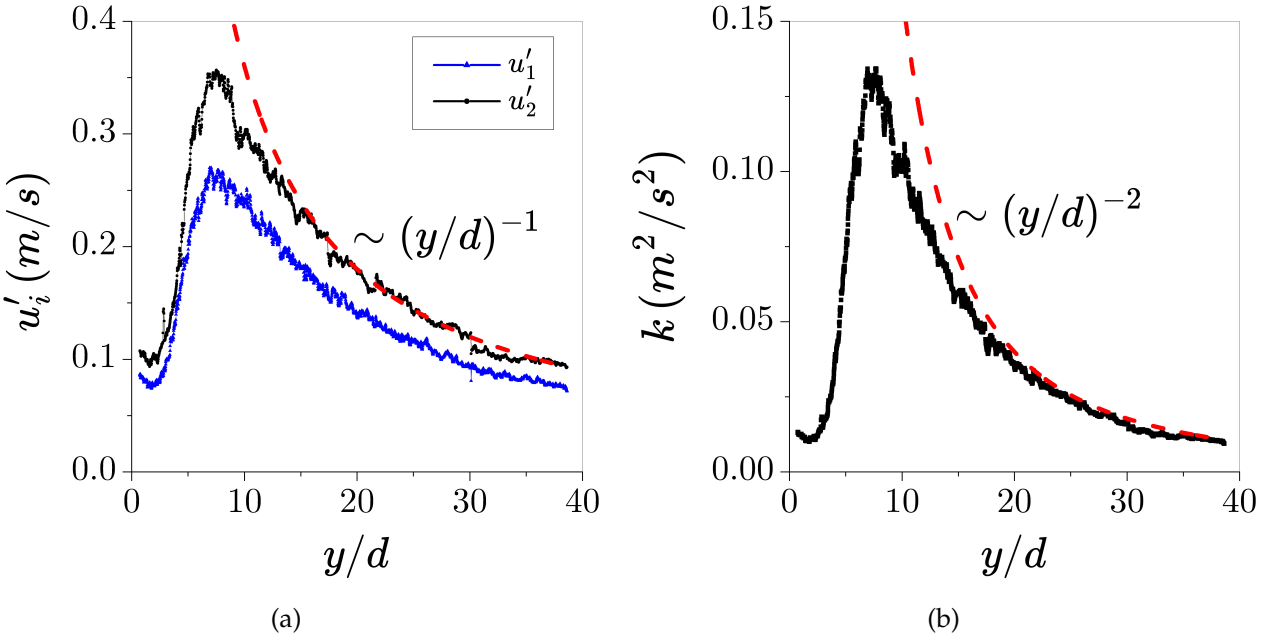


Figure 4. Spatial variation of the time-averaged quantities along the jet centerline (a) root mean square of the turbulence velocity fluctuations in two directions and (b) turbulent kinetic energy.

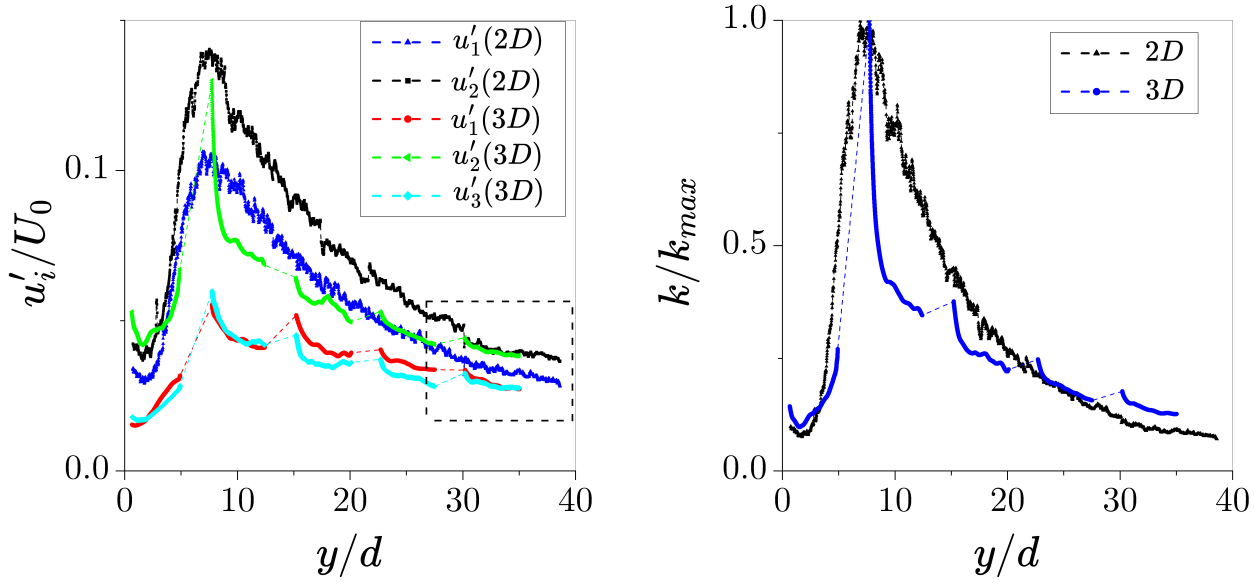


Figure 5. Normalized time-averaged quantities along the jet centerline obtained from planar PIV (2D) and tomographic PIV (3D): (a) RMS of turbulent velocity fluctuations, and (b) turbulent kinetic energy. The dashed lines indicate the region with an agreement between 2D and 3D measurements.

3.2. Turbulent dissipation rate

Following Kolmogorov's similarity hypothesis, the turbulent dissipation rate is defined as

$$\varepsilon = 2\nu\langle s_{ij}s_{ij}\rangle \tag{2}$$

where ν is the kinematic viscosity, $s_{ij} = \frac{1}{2}(\frac{\partial u_i}{\partial x_j} + \frac{\partial u_j}{\partial x_i})$ is the fluctuation strain rate tensor (Pope, 2000). All nine components of the velocity gradient tensor $(\frac{\partial u_i}{\partial x_j})$ are required for dissipation rate computation, which are available in the tomographic PIV. However, in 2D PIV measurements, only four of the nine gradient components are directly accessible. For incompressible flows, the remaining out-of-plane component $\frac{\partial u_3}{\partial x_3}$ can be obtained using the divergence-free assumption. Furthermore, Doron et al. (2001) demonstrated that the dissipation rate within the measurement plane can be estimated under the assumption of local isotropy as follows:

$$\varepsilon = \nu\Big\langle 4(\frac{\partial u_1}{\partial x_1})^2 + 4(\frac{\partial u_2}{\partial x_2})^2 + 3(\frac{\partial u_1}{\partial x_2})^2 + 3(\frac{\partial u_2}{\partial x_1})^2 + 4(\frac{\partial u_1}{\partial x_1}\frac{\partial u_2}{\partial x_2}) + 6(\frac{\partial u_1}{\partial x_2}\frac{\partial u_2}{\partial x_1})\Big\rangle \tag{3}$$

Figure 6(a) shows the variation of the turbulent dissipation rate as a function of normalized distance along the jet centerline. The data points represent experimental measurements, while the red dashed curve indicates the theoretical scaling trend mentioned in previous studies (Viggiano et al., 2021; Antonia et al., 1980; Thiesset et al., 2014). An alignment between experimental data and scaling trend is observed in the far field region, $20 < x/y < 40$.
Figure 6(b) presents the normalized turbulent dissipation rate along the centerline for 2D PIV (black curve) and tomographic PIV (blue curve). The comparison highlights that spatial resolution plays a crucial role even in the far field, where one expects reduced sensitivity. Therefore, achieving reliable far field measurements in the HIT box configuration requires enhanced spatial resolution.

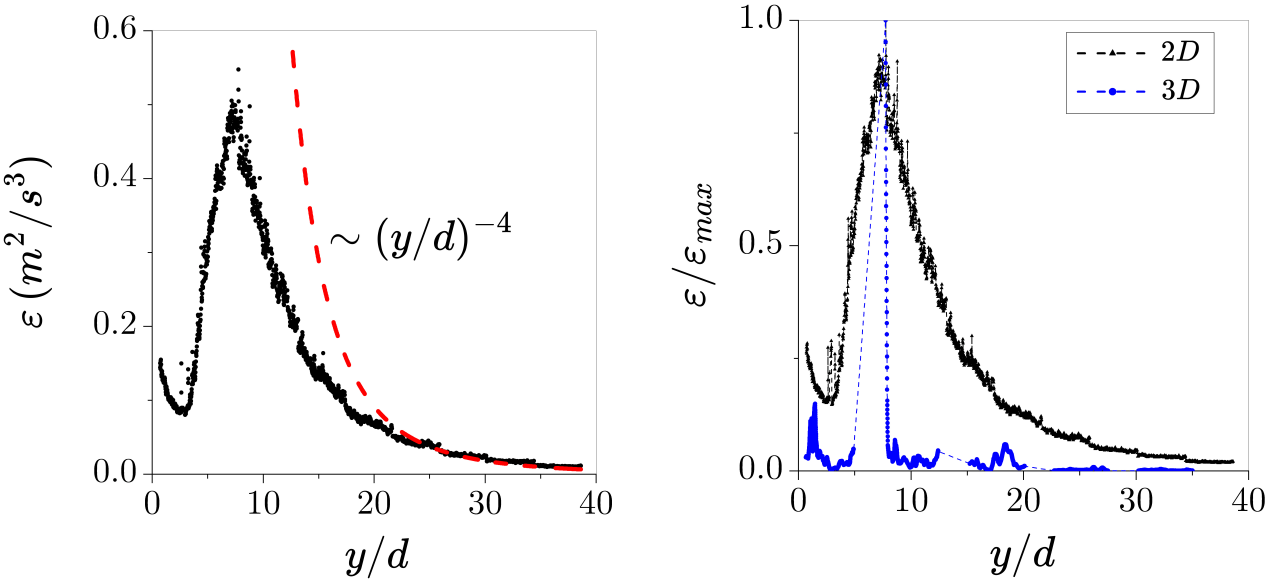


Figure 6. (a) Variation of the turbulent dissipation rate along the centerline, and (b) normalized dissipation rate values from the 2D PIV compared with the tomographic PIV .

3.3. Turbulence decay time scale

A fundamental characteristic of turbulent flows is the large-scale eddy turnover time, which is also known as turbulence decay time scale (Karimpour & Venayagamoorthy, 2013), and is associated with the energy cascade (Apostolidis et al., 2022). This time scale could be approximated with the ratio of k and ε as

$$\tau \equiv \frac{k}{\varepsilon} \tag{4}$$

As discussed earlier in the previous sections, the evolution of turbulent kinetic energy and dissipation rate at the centerline in the far field follows the theoretical power-law scaling. Consequently, it is assumed that the turbulent decay time scale exhibits a similar behavior. Based on equation 4, the corresponding trend line is expressed as $(y/d)^2$. Figure 7 indicates that the trend line must be shifted by a constant value. With this adjustment, the variation of the turbulent decay time aligns with the expected scaling behavior in the far field region ($15 < y/d < 40$). This constant turbulent time scale value C corresponds to the characteristic time scale of the eddy turnover time where the shear layers meet each other along the centerline, leading to intense mixing. In this region, both the turbulent kinetic energy and the dissipation rate reach their maximum values. The location of this interaction zone is highlighted by the red rectangular zone in the contour plots of kinetic energy and dissipation rate in Figure 8. This observation, particularly in the far field region ($30 < y/d < 40$), is useful for the design of an experimental facility based on randomly actuated jet arrays. Further elaboration of the physical meaning of this time scale remains the subject of ongoing work.

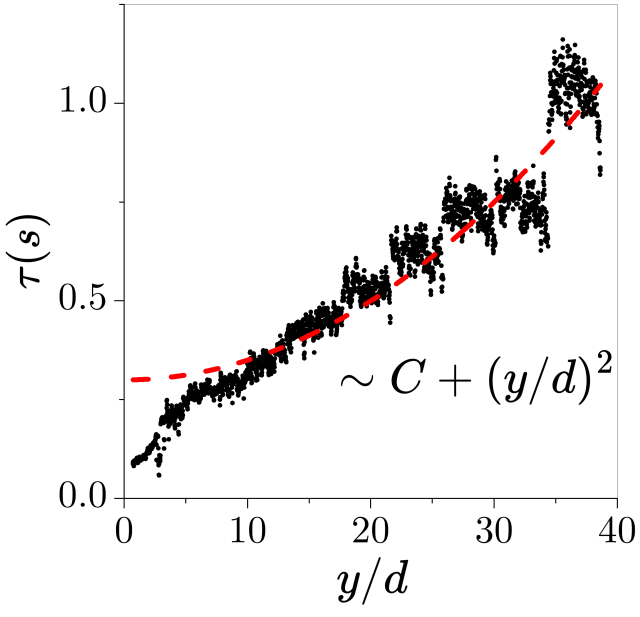


Figure 7. Spatial variation of the time-averaged turbulent decay time scale along the jet centerline.

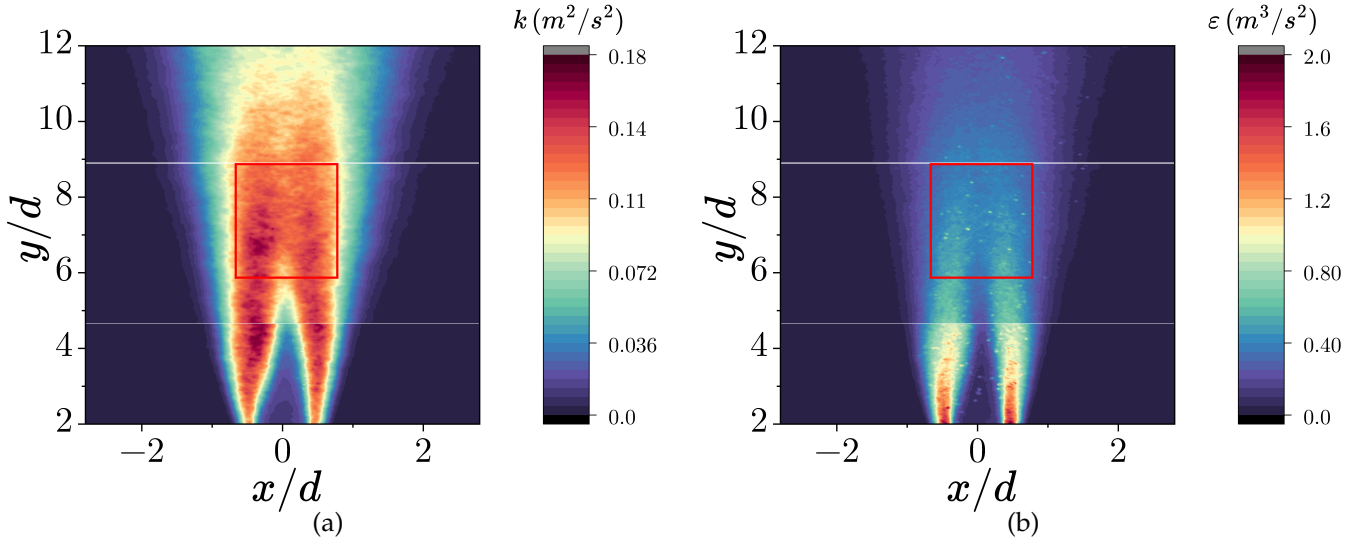


Figure 8. The contours of (a) turbulent kinetic energy, and (b) turbulent dissipation rate in the near field. The red box indicates the region of strong mixing where the peak values of these turbulent quantities occur.

3.4. Spectral Analysis

The high temporal resolution through time-resolved tomographic PIV provides three-dimensional velocity fields at sampling rates sufficient to resolve a wide range of turbulent motions. This temporal fidelity enables the accurate computation of the Power Spectral Density (PSD) of the flow, derived from the of turbulence velocity fluctuations (Beresh, 2021; Ma et al., 2014). To evaluate the feasibility of identifying the turbulent decay power law, the PSD of velocity fluctuations was extracted at four points on the centerline.

Figure 9 presents the Power Spectral Density of the second velocity fluctuation component (u_2) at the selected centerline locations. The black curve corresponds to the near field position at $y/d = 1.1$, close to the nozzle outlet. The red curve represents the location $y/d = 11.6$, placed downstream of the high mixing region highlighted in Figure 8. The green and blue curves correspond to the far field positions where the flow follows self-similar behavior in turbulent kinetic energy, dissipation rate, and turbulent decay time scale. The gray reference line in this figure denotes the $-5/3$ Kolmogorov slope at $y/d = 34.1$, by using Taylor´s frozen hypothesis ($\kappa = 2\pi f/U_c$) defined by the relation

$$E(f) = C_k \varepsilon^{2/3} \left(\frac{2\pi}{U_c}\right)^{-5/3} f^{-5/3} \tag{5}$$

where, C_k is the Kolmogorov constant, U_c is the mean velocity, ε denotes the mean turbulent dissipation rate, and f is the frequency. C_k is taken as 0.51, following the definition provided by (Sreenivasan, 1995). The inclination of the PSDs to $-5/3$ slope at the farther positions indicates

the emergence of an inertial sub-range associated with the fully developed turbulence, whereas the deviation from this slope at positions closer to the jet outlet implies that the flow is still dominated by large-scale coherent structures. These results demonstrate the capability of the tomographic PIV with high temporal resolution as a tool for spectral analysis. This robustness is essential for future investigations within the HIT region, where high-fidelity spectral analysis on vorticity and enstrophy dynamics is required.

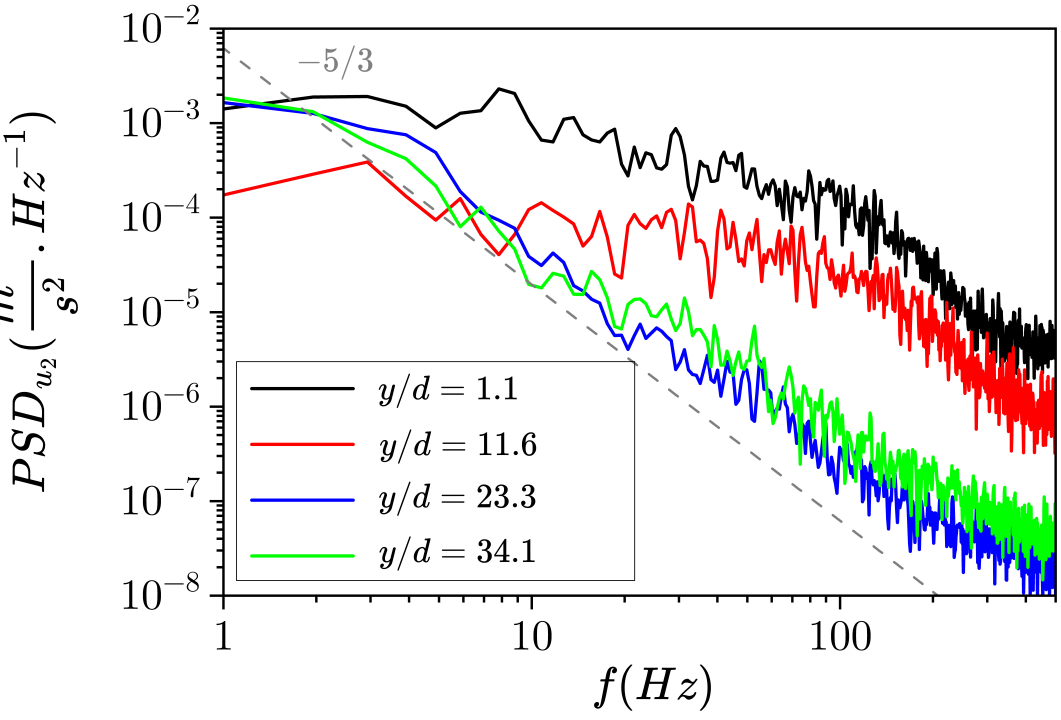


Figure 9. The power spectral density of u_2 component measured with the tomographic PIV along the centerline at four downstream locations: $y/d = 1.1$ (black),11.6 (red), 23.3 (blue) and 34.1 (green). The gray dashed line indicates the $-5/3$ slope.

4. Conclusion

The turbulent characteristics of a single round jet were examined using 2D and tomographic PIV. To evaluate the robustness of these two measurement techniques for characterizing turbulence statistics and performing spectral analysis, a high spatial resolution 2D PIV system and a high temporal resolution tomographic PIV system were employed. The respective resolutions were selected with explicit reference to the relevant Kolmogorov scales. It should be noted that the 2D PIV results rely on assumptions such as local isotropy, divergence-free conditions, and equal velocity

fluctuations in the non-streamwise components.
Mean turbulent kinetic energy, turbulent dissipation rate, and turbulence decay time scale were extracted as results from the time-resolved velocity fields. These parameters were evaluated along the jet centerline over an extended downstream distance of up to forty times the nozzle diameter from the jet outlet. This measurement range captures both the near field region and the fully developed self-similar region of the jet. The results demonstrated that, along with the centerline, the assumption of equality for the root mean square velocity of the turbulent fluctuations in non-streamwise components is not incorrect. Also, the result of tomographic PIV reveals that even without having high spatial resolution in the far field, the measured values converge to 2D PIV results.
The parameter most influenced by spatial resolution is the turbulent dissipation rate, which is highly sensitive to small-scale velocity gradients. The tomographic PIV measurements indicate that, due to the limited spatial resolution of the system in the current experiment, the dissipation is systematically underestimated, and the resulting values are therefore not comparable to the 2D PIV estimates. This outcome highlights the need to increase the spatial resolution in tomographic PIV for future HIT box experiments to ensure reliable measurements of dissipation rate.
To evaluate the consistency of the measured results, the turbulent properties were extracted along the centerline and compared with the self-preservation behavior reported in previous investigations. Experimental observations for turbulent properties in the far field region are in agreement with theoretical scalings reported for $20 < y/d < 40$ and show consistency with the well known -5/3 scaling for fully developed turbulence. Within the scope of this study, these findings provide valuable insights for the design of the HIT box facility in the laboratory using randomly actuated jet arrays, and the associated turbulence statistics required for the droplet fragmentation.

Acknowledgments

This work is supported by ERC grant (FragTuRe, Grant Agreement No.101160908). Funded by the European Union. Views and opinions expressed are, however, those of the author(s) only and do not necessarily reflect those of the European Union or the European Research Council Executive Agency. Neither the European Union nor the granting authority can be held responsible for them.

References

Antonia, R. A., Satyaprakash, B. R., & Hussain, A. K. M. F. (1980). Measurements of dissipation rate and some other characteristics of turbulent plane and circular jets. *Physics of Fluids*, *23*, 695-700.

Apostolidis, A., Laval, J., & Vassilicos, J. (2022). Scalings of turbulence dissipation in space and time for turbulent channel flow. *Journal of Fluid Mechanics*, *946*, A41.

Ball, C., Fellouah, H., & Pollard, A. (2012). The flow field in turbulent round free jets. *Progress in Aerospace Sciences*, *50*, 1-26.

Beresh, S. J. (2021). Time-resolved particle image velocimetry. *Measurement Science and Technology*, *32*(10), 102003.

Doron, P., Bertuccioli, L., Katz, J., & Osborn, T. R. (2001). Turbulence characteristics and dissipation estimates in the coastal ocean bottom boundary layer from PIV data. *Journal of Physical Oceanography*, *31*, 2108–2134.

George, W. K. (1989). The self-preservation of turbulent flows and its relation to initial conditions and coherent structures. In W. K. George & R. E. A. Arndt (Eds.), *Advances in turbulence* (pp. 39–73). Hemisphere.

Hassanzadeh, H., & Taghavi, S. M. (2024). A review on free miscible buoyant jets. *Physics of Fluids*, *36*, 061301.

Karimpour, F., & Venayagamoorthy, S. K. (2013). Some insights for the prediction of near-wall turbulence. *Journal of Fluid Mechanics*, *723*, 126–139.

Kewalramani, G., Ji, B., Dossmann, Y., Becker, S., Gradeck, M., & Rimbert, N. (2024). A simple analytical model for turbulent kinetic energy dissipation for self-similar round turbulent jets. *Journal of Fluid Mechanics*, *983*, A44.

Lipari, G., & Stansby, P. K. (2011). Review of experimental data on incompressible turbulent round jets. *Flow, Turbulence and Combustion*, *87*, 79–114.

Ma, X., Geisler, R., Agocs, J., & Schröder, A. (2014). Time-resolved tomographic piv investigation of turbulent flow control by vortex generators on a backward-facing step. In *Proceedings of the 17th international symposium on applications of laser techniques to fluid mechanics, lisbon, portugal.*

Pope, S. (2000). *Turbulent flows*. Cambridge University Press.

Sreenivasan, K. R. (1995). On the universality of the kolmogorov constant. *Physics of Fluids*, *7*(11), 2778–2784.

Thiesset, F., Antonia, R., & Djenidi, L. (2014). Consequences of self-preservation on the axis of a turbulent round jet. *Journal of Fluid Mechanics*, *748*, R2.

Viggiano, B., Basset, T., Solovitz, S., Barois, T., Gibert, M., Mordant, N., … Cal, R. B. (2021). Lagrangian diffusion properties of a free shear turbulent jet. *Journal of Fluid Mechanics*, *918*, A25.

Xu, G., & Antonia, R. (2002). Effect of different initial conditions on a turbulent round free jet. *Experiments in Fluids*, *33*, 677-683.